ISSN 2706-655X Vol. 7, Issue 3: 101-110, DOI: 10.25236/IJFET.2025.070314

Research on Sliding Mode Active Disturbance Rejection Control Strategy of CLLC Resonant Converter

Siwen Qi

Faculty of Electrical and Control Engineering, Liaoning Technical University, Huludao, 125105, Liaoning, China

Abstract: *The CLLC full-bridge resonant converter suffers from slow response speed, poor dynamic performance and poor interference immunity when compensated by traditional control strategies, and this paper proposes a composite control strategy based on improved sliding mode self-immunity. Firstly, a nonlinear model of the CLLC full-bridge resonant converter is established by the extended function description method, and the system is fitted using the frequency sweep method. Secondly, the self-immunity linear extended observer is designed to estimate and compensate the error, the super-helix sliding mode algorithm is used to replace the traditional error feedback control law in self-immunity, the self-immunity error feedback control rate is optimised, and the sliding mode surface and super-helix sliding mode structure are improved, and once again, the jitter vibration phenomenon of the system is effectively reduced by using the smoothed sigmoid function instead of the discontinuous sign function. After that, the parameters of the controller are optimised by PSO algorithm to improve the stability of the system. Finally, the effectiveness of the improved super-helical sliding mode self-immunity control strategy is verified by simulation and experimental analysis. The results show that the strategy effectively improves the problems of output voltage overshooting and long regulation time of the traditional PI controller in the case of sudden change, and has good dynamic performance and robustness.*

Keywords: *CLLC Resonant Converter; Soft Switching; Self-Turbulence Control; Sliding Mode Control; Dynamic Response*

1. Introduction

The transition to sustainable clean energy has become an urgent global necessity[1,2]. Nevertheless, renewable energy sources like solar and wind power are often hindered by environmental factors such as light intensity and wind speed, leading to unstable and intermittent energy production [3]. To mitigate these fluctuations and enhance system stability, energy storage devices are essential in such systems. From a microgrid's structural perspective[4], DC-DC converters are crucial in ensuring the quality and stability of the electrical energy by regulating the voltage between different power sources and loads, while also optimizing energy efficiency [5]. Therefore, researching high-efficiency DC-DC converters is vital for improving energy system performance.

To improve the reliability of on-board power supplies, the converter must have faster response times and enhanced anti-interference capabilities [13]. This makes closed-loop control of the converter particularly crucial. Research on resonant converter closed-loop control strategies has largely focused on PID control. For example, literature [14] combines PID control with optimal trajectory control, proposing a composite strategy that switches between the two control modes based on load changes, thereby improving the converter’s dynamic response to sudden load fluctuations. Literature [15] introduces a hybrid integral sliding mode-PI control strategy using a fuzzy algorithm, which ensures a smooth transition between integral sliding mode-PI control and PI control, enhancing the system's response to sudden variations in load and input voltage, while minimizing error. Z. Xia et al. [16] propose a seamless cooperative control strategy integrated with the widely used proportional-integral (PI) control in fixed-peak mode, enabling optimal switching modes for fast and smooth dynamic transitions under constant peak resonant current conditions. Chen H. et al. [17] introduce a novel deadband-based constant current control method, which directly and effectively controls the charging and discharging of the output capacitor—something traditional PI control cannot achieve.

ISSN 2706-655X Vol. 7, Issue 3: 101-110, DOI: 10.25236/IJFET.2025.070314

However, since PID control requires highly accurate modeling of the controlled system, and the CLLC resonant converter cannot be precisely modeled due to its high-order characteristics, achieving ideal control performance across the entire frequency range remains challenging.

To address these challenges, literature [18] introduces an Active Disturbance Rejection Control (ADRC) strategy for LLC resonant converters, which significantly enhances the system's stability and robustness. However, if the disturbance's characteristics or amplitude vary greatly, it could negatively affect the control system's performance. Literature [19] presents a higher-order sliding mode control (SMC) design approach. The sliding mode surface, derived from the output voltage characteristics of the CLLC converter, incorporates higher-order derivatives of voltage and current, along with an error integral term for the output voltage. Samir Abdelmalek et al. [20] propose a new nonlinear robust controller for DC-DC buck converters used in renewable energy MPPT systems, enabling fast and reliable tracking of the output voltage in the DC bus of power supplies. Literature [21] introduces a dual phase shift (DPS) control method based on time-domain analysis, which achieves a wide voltage output range with constant current source characteristics without sacrificing soft switching. Literature [22] presents a sliding mode control technique based on global integral sliding mode, replacing the sign function in switching control with a continuous function to reduce the jitter typically associated with sliding mode control. Literature [23] discusses discrete pulse frequency modulation for sliding mode control, deriving the sliding surface through input-output linearization to achieve a more optimal dynamic response of the output voltage, robust against dynamic drift issues.

2. Topology and operation principle of the converter

2.1 Topology of full bridge CLLC resonant converter

The main topology of the CLLC converter is shown in Figure 1, which contains the high-voltage side power supply V1, the low-voltage side power supply V2, the transformer primary side H1 bridge composed of S1~S4, the transformer secondary side H2 bridge composed of S5~S8, the high-frequency transformer T, as well as the two pairs of resonance networks Lr1, Cr1 and Lr2, Cr2. The converter is mainly composed of two identical H-bridges as well as the LC resonance network and is connected by a high-frequency transformer to form a path. connected by a high-frequency transformer to form a path. The main difference between the CLLC converter and the conventional LLC converter is that the resonant network composed of LCs is added to the vice-side measurements, thus making the forward and reverse topologies identical, so that the energy flow in the forward and reverse directions can be controlled in the same way.

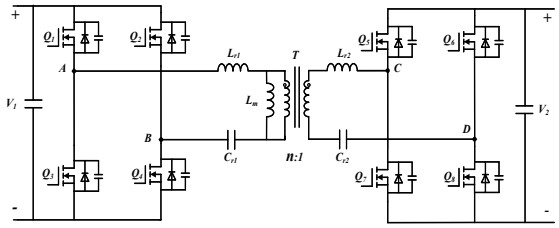

Figure 1 Circuit topology of full-bridge CLLC resonant converter

The CLLC converter resonant network is a series-parallel structure using inductance-capacitance, therefore, there are two resonant frequency points, for example, in forward operation, when only Lr1 and Cr1 participate in the resonance, the resonance frequency is fr; if the excitation inductance Lm participates in the resonance, then the resonance frequency is fm. The two resonance frequencies are defined as Eqs.(1) and Eqs.(2), respectively:

$$f_r = \frac{1}{2\pi\sqrt{L_{r1}C_{r1}}} \tag{1}$$

$$f_m = \frac{1}{2\pi\sqrt{(L_{r1}+L_m)C_{r1}}} \tag{2}$$

According to the two resonance points, the switching frequency fs's can be divided into three intervals, and the three intervals correspond to three kinds of operating conditions [26], when fm<fs<fr, it is the under-resonance condition, when fs=fr, it is the quasi-resonance condition, and when fs >fr, it

ISSN 2706-655X Vol. 7, Issue 3: 101-110, DOI: 10.25236/IJFET.2025.070314

is the over-resonance condition. The CLLC operating frequency must be greater than fm to satisfy the soft-switching condition.

In order to simplify the difficulty of system analysis, according to its operating characteristics, the fundamental wave analysis method is used for the circuit equivalent of the CLLC converter. The equivalent circuit of CLLC is shown in Figure 2.

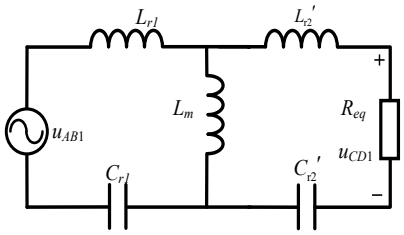

Figure 2 CLLC equivalent circuit diagram

According to the equivalent circuit, the system DC voltage gain curve, i.e., DC gain M, can be obtained:

$$M(f_n)=\|H,(f_n)\|=\frac{1}{\sqrt{\left(\frac{Q}{k}\right)^2\left((2k+1)f_n-\left(\frac{2k+2}{f_n}\right)+\frac{1}{f_n^2}\right)^2+\left(1+\frac{1}{k}-\frac{1}{k}f_n^2\right)^2}} \tag{3}$$

In the equation, Q is the quality factor, Req is the equivalent load, $Q=\frac{\sqrt{Lr}}{Cr}/R_{eq}$, k is the inductance ratio k=Lm/Lr, and fn is the normalized frequency fn=fs/f.

According to Eq. (3), it can be seen that the size of the gain M is related to the values of k and Q. Taking the selection of Q=0.4 and k=5 as an example, the change rule of the gain with the value of k versus the normalized frequency and the change rule of the gain with the value of Q versus the normalized frequency can be obtained as shown in Figure 3 (a) and (4).

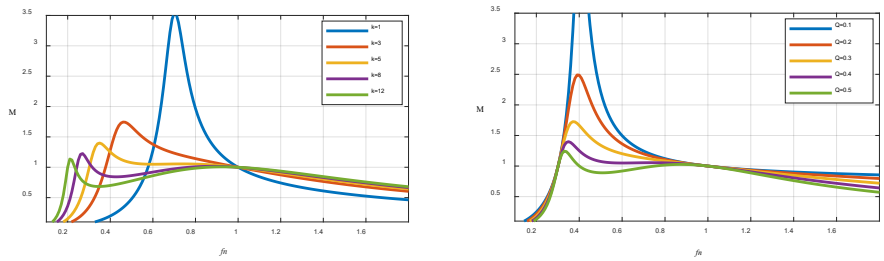

(a)Effect of k *(b) effect of Q*

Figure 3 Effect of k and Q

When the k value is small, the frequency variation range is narrower, making the controller regulation more sensitive. However, too small a value of k causes the excitation inductance Lm to decrease and increases the current through Lm, which leads to an increase in the excitation inductance loss and reduces the conversion efficiency. On the other hand, a smaller Q value results in a larger peak voltage gain, but it also implies a wider range of switching frequency variations in the converter, making the regulation frequency range too large, which leads to a longer regulation time. Therefore, weighing the inductance ratio and quality factor, the quality factor Q=0.23, inductance ratio k=6 are selected as the design parameters of the converter.

2.2 Analysis of the small-signal model for the CLLC resonant converter

In order to meet system analysis and design requirements, isolated high-frequency DC/DC converters are often modeled using the extended function description method. This method more accurately characterizes the dynamics of the converter and provides a more reliable model by considering the case where the resonant frequency is close to the switching frequency.

The small-signal model of a CLLC resonant converter can be described as:

ISSN 2706-655X Vol. 7, Issue 3: 101-110, DOI: 10.25236/IJFET.2025.070314

$$\begin{cases} \dfrac{d\hat{x}}{dt} = A\hat{x} + B\hat{u} \\ \hat{y} = C\hat{x} \end{cases} \tag{4}$$

In the equation, A, B, and C are coefficient matrices, determined by the actual parameters of the topology, the transfer function describing the switching frequency perturbation corresponding to the output voltage fluctuation is written as:

$$G(s) = \frac{\hat{u}_o(s)}{\hat{f}_s(s)} = C(sI - A)^{-1} B \tag{5}$$

The amplitude-phase characteristic curves of the EDF small-signal model, the fitted low-order equivalent model, and the swept-frequency data points are given in Figure 4.

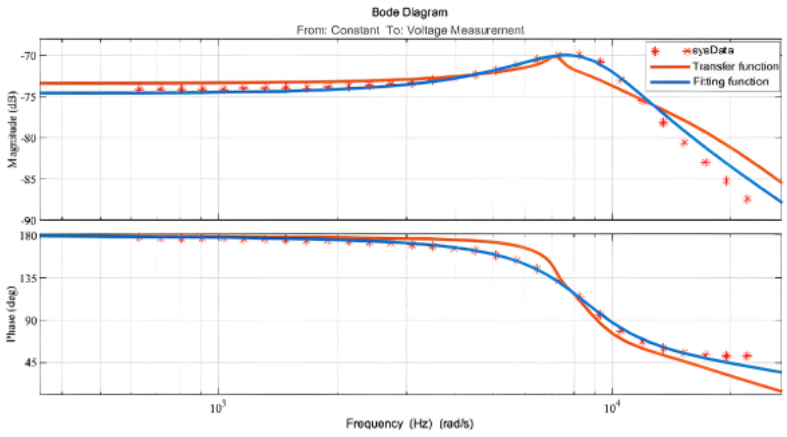

Figure 4 Function fitting image

Comparison shows that the EDF small-signal model and the MATLAB power model sweep fitted low-order equivalent model have errors in the high-frequency band, while in the low-frequency band and the mid-frequency band has a high fitting accuracy. The transfer function fitted from the data results of the above power model sweep is:

$$G(s) = \frac{-0.4638s - 1.484\times10^4}{s^2 + 5812s + 7.716\times10^7} \tag{6}$$

3. Self-immunity control and sliding mode control controller design

3.1 Principle of linear self-immunity control

Self-immunity control is an active anti-disturbance control method, and its core idea is to eliminate the internal and external uncertainty disturbances of the controlled object through the control signal, so as to reduce the interference of external disturbances on the controlled object. The basic structure of linear self-immunity control is shown in Figure 5.

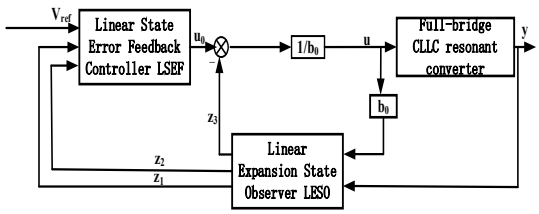

Figure 5 Second-order linear ADRC control structure diagram

Figure 5 shows the control block diagram of the CLLC system based on linear ADRC. In ADRC controller, the expansion observer is the central part. It considers the total perturbation as a new state variable and constructs the state equations of the controlled object by means of the outputs, the differentiation of the outputs and the perturbations. Reducing the system and the dilation observer to the form of an integrator simplifies the design of the feedback control rate.

ISSN 2706-655X Vol. 7, Issue 3: 101-110, DOI: 10.25236/IJFET.2025.070314

3.2 Design of expansion state observer

Based on the above modeling of the CLLC converter, specifically the results from the reduced-order approximation, it can be inferred that the CLLC converter can be analyzed using the equivalent approach of a second-order ADRC. The typical differential equations for a second-order controlled system are presented in Eq. (7).

$$\ddot{y} = f\left(y, \dot{y}, \omega(t), t\right) + b_0 u \tag{7}$$

In the equation, ω(t) denotes the perturbation caused by external factors, and f denotes the total perturbation caused by the system both internally and externally Let , $x_1 = y$, $x_2 = \dot{y}$, $x_2 = \ddot{y}$ be the state variables, and the system spatial state expression is shown in Eq. (8).

$$\begin{cases} \begin{bmatrix} \dot{x}_1 \\ \dot{x}_2 \\ \dot{x}_3 \end{bmatrix} = \begin{bmatrix} 0 & 1 & 0 \\ 0 & 0 & 1 \\ 0 & 0 & 0 \end{bmatrix} \begin{bmatrix} x_1 \\ x_2 \\ x_3 \end{bmatrix} + \begin{bmatrix} 0 \\ b_0 \\ 0 \end{bmatrix} u + \begin{bmatrix} 0 \\ 0 \\ 1 \end{bmatrix} \dot{f} \\ y = \begin{bmatrix} 1 & 0 & 0 \end{bmatrix} \begin{bmatrix} x_1 \\ x_2 \\ x_3 \end{bmatrix} \end{cases} \tag{8}$$

To estimate x_1, x_2, and x_3, the control object can be linearly expanded observer as follows:

$$\begin{cases} \dot{z} = Az + Bu + L\left(x_1 - z_1\right) \\ \hat{y} = Cz \end{cases} \tag{9}$$

In the equation, L is the observer error gain matrix, C is the unit matrix, whose matrix is expressed as $L = [\beta_1 \quad \beta_2 \quad \beta_3]^T$ where β_1, β_2, β_3 are the error gain, which leads to the LESO space state expression:

$$\begin{cases} \begin{bmatrix} \dot{z}_1 \\ \dot{z}_2 \\ \dot{z}_3 \end{bmatrix} = \begin{bmatrix} -\beta_1 & 1 & 0 \\ -\beta_2 & 0 & 1 \\ -\beta_3 & 0 & 0 \end{bmatrix} \begin{bmatrix} z_1 \\ z_2 \\ z_3 \end{bmatrix} + \begin{bmatrix} 0 & \beta_1 \\ b_0 & \beta_2 \\ 0 & \beta_3 \end{bmatrix} u + \begin{bmatrix} 0 \\ 0 \\ 1 \end{bmatrix} \begin{bmatrix} u \\ y \end{bmatrix} \\ \hat{y} = \begin{bmatrix} 1 & 0 & 0 \\ 0 & 1 & 0 \\ 0 & 0 & 1 \end{bmatrix} \begin{bmatrix} z_1 \\ z_2 \\ z_3 \end{bmatrix} \end{cases} \tag{10}$$

In the equation, z_1, z_2, z_3 are the dilated state observer states, and the observations and total perturbations of the dilated state observer are compensated to the controller, then the state error feedback control is set up as in Eq. (11), with a control quantity of u_0.

$$u = \frac{k_p(r - z_1) - k_d z_2 - z_3}{b_0} = \frac{u_0 - z_3}{b_0} \tag{11}$$

In the equation, r is the given value. When the controller is running normally, z_1 gradually converges to the output value y, z_2 gradually converges to the output value of the first-order differential, z_3 gradually converges to the perturbation f, therefore, the second-order differential equation of the controlled object is converted to the form shown in Eq. (12):

$$\ddot{y} = k_p\left(r - z_1\right) - k_d z_2 - z_3 + f = u_0 \tag{12}$$

To maintain the stability of the system, the observer's characteristic polynomial poles and the closed-loop characteristic polynomial poles are configured at the observer bandwidth ω_o and the controller bandwidth ω_c, respectively. By transforming ω_o, the error feedback coefficients as shown in Eq. (13) can be obtained.

$$\lambda(s) = \left|sI - (A - LC)\right| = \left(s + \omega_0\right)^3 \tag{13}$$

In the equation, I is the unit matrix, therefore, the gain matrix is only related to the bandwidth of the observer, which makes the design of the linear expansion observer simple. The controller parameters satisfy the following relationship:

ISSN 2706-655X Vol. 7, Issue 3: 101-110, DOI: 10.25236/IJFET.2025.070314

$$\begin{cases} \beta_1 = 3\omega_0, \ \beta_2 = 3\omega_0^2, \ \beta_3 = \omega_0^3 \\ k_p = \omega_c^2, k_d = 2\omega_c \end{cases} \tag{14}$$

In the equation, ω_c is the bandwidth of the controller. After the design of the linear dilated state observer and the linear error feedback control rate, the LADRC's rectification parameters become three, which are the bandwidth of the observer ω_o, the bandwidth of the controller ω_c, and the control volume gain b_0.

3.3 Principle of super-helical sliding mode self-resilient control

Sliding-mode control is a variable-structure control strategy that achieves stable control of a system by introducing a sliding surface. The structure of the sliding mode self-immunity control is shown in Figure 6.

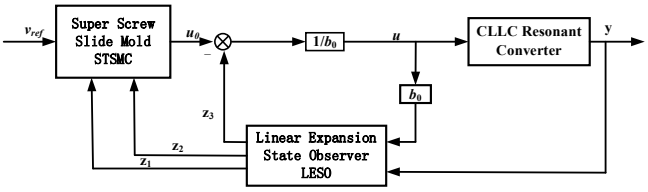

Figure 6 Structure of super-helical sliding mode self-immunity controller

The sliding mode self-immunity control is composed of two components, the sliding mode controller and the linear expansion state observer, and the core of the whole control structure is the self-immunity control, while the sliding mode surface and the sliding mode control law based on the exponential convergence law are introduced in the error feedback control law in order to improve the dynamic performance and steady state performance of the system.

3.4 Improved super-helical sliding mode self-immunity controller design

In this paper, the sliding mode surface is defined as shown in Eq. (15).

$$s = ce + \dot{e} \tag{15}$$

In the equation, c is the adjustable parameter, e is the tracking error, $\dot{e}$ is the derivative of the tracking error, and the error is defined as $e = x_1 - V_{ref}$, Vref is the output reference voltage. In order to improve the response speed of the control system, let c satisfy Eq. (16).

$$c = \begin{cases} \lambda, |e| > 1 \\ \lambda |e|^n, 0 \le |e| \le 1 \end{cases} \tag{16}$$

In the equation, λ and k are constants greater than 0 and n is a constant greater than or equal to 1. The differentiation to find s is shown in Eq. (17).

$$\dot{s} = c\dot{e} + \ddot{e} = cx_2 + \left(f + b_0 u\right) \tag{17}$$

The Super-Twisting Sliding Mode Control (STSMC) algorithm is a special high-order sliding mode control technique, which quickly realizes the convergence of the system state through the dynamic rotational trajectory, significantly reduces the jitter and ensures the smoothness of the control process.The STSMC control algorithm can be written down in the following form:

$$\begin{cases} \dot{s} = -\lambda |s|^r \cdot sign(s) + v \\ \dot{v} = -\alpha \cdot sign(s) \end{cases} \tag{18}$$

In the equation, λ and α are gain coefficients, sign(s) is the sign function, and r is the coefficient to be designed, generally taken as 0.5.

The curve-smoothing sigmoid function is used instead of the sign function, which simplifies the design of the controller, improves the efficiency of the control output, and enables the CLLC resonant

ISSN 2706-655X Vol. 7, Issue 3: 101-110, DOI: 10.25236/IJFET.2025.070314

converter to realize dynamic regulation through fewer digital logic resources. Sigmoid function provides continuous control signals and reduces the frequent switching of the control inputs, which effectively reduces the jittering phenomenon of the system and improves the stability of the control process. The expression is:

$$sigmoid(s)=\frac{s}{|s|+\sigma} \tag{19}$$

The improved super-helix control algorithm can be obtained as:

$$\begin{cases}\dot{s}=-\lambda|s|^{r}\cdot sigmoid(s)+v\\ \dot{v}=-\alpha\cdot sigmoid(s)\end{cases} \tag{20}$$

From Eqs. (17) and (20), the sliding mode self-resistant controller can be designed as:

$$u=-\frac{1}{b_0}\left(cx_2+f+\lambda|s|^{\frac{1}{2}}\cdot sigmoid(s)-v\right) \tag{21}$$

To analyze its stability, the Lyapunov function $V=s^2/2$ is taken as the determining condition, and its derivation and substitution of the convergence law can be obtained as follows:

$$\begin{aligned}&\dot{V}=s\dot{s}\\&=\dot{s}\left(cx_2+b_0u+f\right)\\&=s\left[cx_2+\omega+\lambda|s|^{\frac{1}{2}}\cdot sigmoid(s)-v\right]\\&=-\lambda|s|^{\frac{1}{2}}\frac{s^2}{|s|+\sigma}-\alpha\int\frac{s^2}{|s|+\sigma}d(t)\end{aligned} \tag{22}$$

Since both k and β are greater than 0, so $\dot{V}<0$. According to the Liapunov stability theory, it is known that the controller can converge to zero in a finite time. Therefore, the LSMC-ADRC control system is asymptotically stable.

3.5 Control parameter optimization simulation

The PSO optimization algorithm of controller parameters is written in MATLAB, and then the simulation model of ITAE performance index is added to the simulation model of CLLC resonant converter under STSMC_LADRC control, so that the PSO algorithm and the STSMC_LADRC simulation model are linked to optimize the control parameters. In order to ensure that the parameters can be repeated iteratively, the flow of the PSO algorithm is shown in Figure 7.

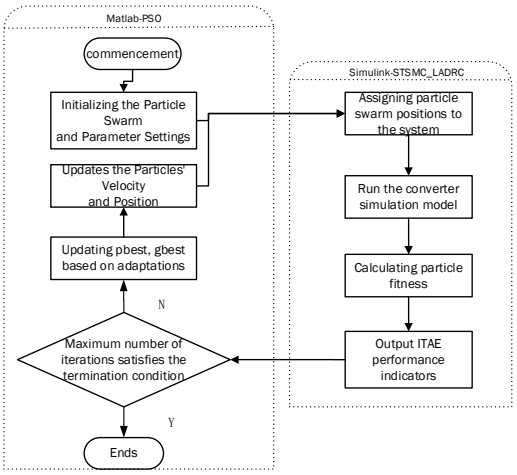

Figure 7 Flow chart of PSO algorithm parameter optimization

To optimize the algorithm, first run the PSO algorithm code of MATLAB, call Simulink simulation model and pay the initial particle swarm position to the CLLC resonant converter under the control of STSMC_LADRC, and the simulation obtains the adapted value to be output to the MATLAB workspace through the out interface. The algorithm then judges the adaptation value, if it does not meet

ISSN 2706-655X Vol. 7, Issue 3: 101-110, DOI: 10.25236/IJFET.2025.070314

the termination conditions, then update the speed and position of the particles, that is, the adjustment parameters, and then sent to the simulation model to run iterations, if it meets the termination conditions, then exit the simulation, to obtain the optimal solution of the STSMC_LADRC control parameter.

4. Experimental verification

The experimental platform mainly includes the following key parts, the resonant converter main circuit, used to realize the voltage conversion, the input voltage is converted into the required output voltage; DSP control circuit, used to sample the output voltage and current of the converter, and through the control program to achieve the control of the converter's original switching tube operating frequency, in order to meet the output requirements; the input side of the DC adjustable power supply, the output voltage range 0~600V, and has an output power of up to 750W; an electronic load on the output side, which can realize stable output and load mutation; an auxiliary power supply, which provides 12V DC in the experimental platform, is used to provide the required power support for the signal side of the DSP and the resonant converter; and a digital oscilloscope, which is used to analyze and record the output waveforms of the load, and the experimental platform is shown in Figure 8.

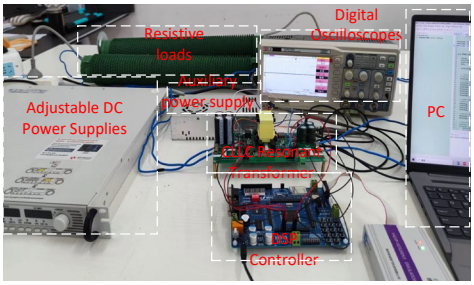

Figure 8 Experimental platform for CLLC resonant converter

The zero-voltage turn-on of the primary switch is tested under the rated input voltage of 480V and full load resistance of. The soft-switching results are shown in Figure 9, with the red curve showing the drain-source voltage V_{ds1} waveform of the primary-side switch S_1 and the blue curve showing the gate signal V_{gs1} waveform of the switch S_1.

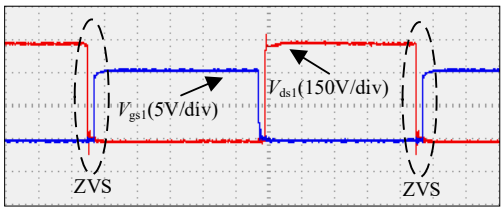

Figure 9 Switching tube soft switching waveform

After the system is stabilized, the resistance value of the load is changed to observe the dynamic performance of the CLLC resonant converter when the load changes abruptly. The output voltage waveforms of the converter when bucking and boosting are shown in Figure 10, and when loading is shown in Figure 11; the load resistance is switched from to when load shedding, i.e.; the load is changed from a full load state to a half load state. This is switched from a half load state to a full load state when loading. As can be seen from the waveform transformation diagram, all three control strategies can make the CLLC resonant converter in the case of sudden changes in the load the system stabilizes the output of 48V voltage.

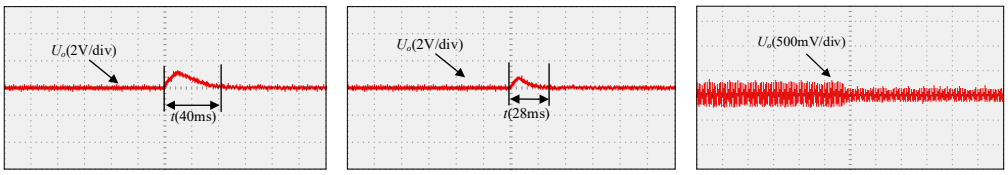

(a) PI *(b) LADRC* *(c) STSMC-LADRC*

Figure 10 CLLC resonant converter load shedding mutation waveforms

ISSN 2706-655X Vol. 7, Issue 3: 101-110, DOI: 10.25236/IJFET.2025.070314

Under the PI control strategy, when the load is lightened, it causes a voltage fluctuation of about 1.6V in the output voltage, and it takes about 40ms to reach the steady state voltage, under the LADRC control, the output voltage will first rise by 0.9V during load shedding, and return to the normal steady-state voltage after 28ms, and the output voltage can always be stabilized near 48V under the STSMC-LADRC strategy.

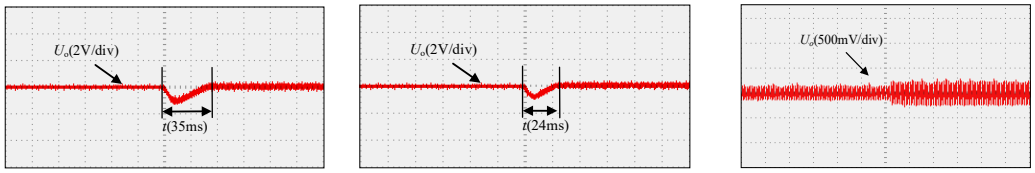

(a) PI *(b) LADRC* *(c) STSMC-LADRC*

Figure 11 CLLC resonant converter loading burst waveforms

Under the PI control strategy, when the load is increased, it causes a voltage fluctuation of about 1.4V in the output voltage, which reaches a steady state after 35ms. Under LADRC control, the output voltage will first drop 0.7V when loading, and recover to the normal steady state voltage after 24ms; under the STSMC-LADRC strategy, the output voltage can always be stabilized near 48V, and the voltage amplitude is about 190mV voltage dither ripple due to the introduction of the super-helical sliding-mode structure and the fact that there is no voltage increment generation when the load is suddenly changed without the need of regulation time.

5. Conclusion

This paper analyzes the operating principle and gain characteristics of the full-bridge CLLC resonant converter, based on which a sliding mode self-immunity based control method for the CLLC resonant converter is proposed for the problem of degradation of control performance due to sudden load change. The effect of the control strategy on the output voltage due to the sudden load change of the converter is analyzed in detail, the model is established by the extended descriptive function method and the equivalent the self-immobilization control structure is designed for the model, and the expanded state observer is used for real-time estimation and compensation of the system, based on which the sliding-mode control structure is added and the exponential convergence law is used for designing the nonlinear state of the self-immobilization control structure. Error feedback control law, and simplified the design of control parameters by bandwidth method. Experimental results show that the control strategy proposed in this paper has good dynamic performance and disturbance suppression ability, improves the overall stability of the system, effectively reduces the output voltage ripple, and meets the demand for faster dynamic response of CLLC converters.

References

[1] P. Prajof, and V. Agarwal. Novel Four-Port DC–DC Converter for Interfacing Solar PV–Fuel Cell Hybrid Sources with Low-Voltage Bipolar DC Microgrids. IEEE J. Emerg. Sel. Top. Power Electron. 2020, 8(2): 1330-1340.

[2] N. P. Santos, et al. Power Management Strategy Based on Virtual Inertia for DC Microgrids. IEEE Trans. Power Electron. 2020, 99: 1.

[3] Q. N. Chen, Research on voltage quality in distributed power supply system. Shanghai: Shanghai University of Electric Power, 2014.

[4] F. Gao, R. Kang, J. Cao, et al. Primary and secondary control in DC microgrids: a review. J. Mod. Power Syst. Clean Energy, 2019, 7(2): 227-242.

[5] J. Wang, K. Sun, H. Wu, et al. Hybrid Connected Unified Power Quality Conditioner Integrating Distributed Generation with Reduced Power Capacity and Enhanced Conversion Efficiency. IEEE Trans. Power Electron. 2020, 68(12): 12340-12352.

[6] P. He, A. Mallik, A. Sankar, et al. Design of a 1-MHz High-Efficiency High-Power-Density Bidirectional GaN-Based CLLC Converter for Electric Vehicles. IEEE Trans. Veh. Technol. 2018, 68: 213-223. DOI: 10.1109/TVT.2018.2881276.

[7] J. Lu, X. Q. Tong, J. X. Zhang, et al. Research on composite optimal trajectory control strategy for L-LLC resonant bi-directional DC-DC converter, J. Electrotechnol. 2020, 35(1): 1-11. DOI: 10.19595/j.cnki.1000-6753.tces.L80393.

[8] Y. Y. Zhao, et al. Integral sliding mode-PI hybrid control of a full-bridge LLC resonant converter.

ISSN 2706-655X Vol. 7, Issue 3: 101-110, DOI: 10.25236/IJFET.2025.070314

Control Eng. 2024, 31(7): 1286-1296. DOI: 10.14107/j.cnki.kzgc.20220458.
[9] Z. Xiao, J. Wu, Z. He, Z. Yao and Y. Tang, Optimal Switching Pattern Control of the CLLC Resonant Converters in Dynamic Processes, IEEE Trans. Power Electron. 2024, 39(12): 16268-16282. DOI: 10.1109/TPEL.2024.3457899
[10] H. Chen, K. Sun, L. Lu, S. Wang and M. Ouyang, A Constant Current Control Method with Improved Dynamic Performance for CLLC Converters, IEEE Trans. Power Electron. 2022, 37(2) 1509-1523. DOI: 10.1109/TPEL.2021.3108631.
[11] X. C. Zong et al. Study on charge self-immunity control strategy for LLC resonant converter. J. Power Sources. 2024, 26(8): 1-12.
[12] L. X. Wang, W. G. Luo, D. Hung. Research on Automotive Bidirectional CLLC Resonant Converters Based on High-Order Sliding Mode Control. Electronics Newsweekly. 2022, 11(18): 26-30.
[13] S. Abdelmalek, A. Dali, A. Bakdi and M. Bettayeb, Design and experimental implementation of a new robust observer-based nonlinear controller for DC-DC buck converters, Energ. 2022, 213: 118816.
[14] D. Wang, L. Zhao, M. Chang, et al, Dual-Phase Shifting Strategy for CLLC Resonant Converters Electr. Eng. Technol. 2024, 19: 2347–2360 . https://doi.org/10.1007/s42835-023-01755-x.
[15] Y. Liu, B. Wang, et al, Sliding mode control of LLC resonant converter for electric vehicle on-board power supply. J. Electr. Mach. Control, 2020, 24(3): 131-137.
[16] H. Ma, Q. Liu, Y. Wang. Discrete pulse frequency modulation control with sliding-mode implementation on LLC resonant DC/DC converter via input–output linearization , IET Power Electron. 2024, 7(5): 1033-1043 .
[17] H. Du, M., et al. Design of self-immunity speed regulation system for permanent magnet synchronous motor with super-helical sliding mode. J. Chongqing Univ. Technol. (Nat. Sci.) 2022, 36(10): 216-222.
[18] C. L. Li, et al. Sliding mode self-immunity control of SIDO Buck converter based on high-order filtered super-helix ESO. J. Shanghai Jiao Tong Univ. 2024, 20(1): 1-24. DOI: 10.16183/j.cnki. jsjtu. 2024. 043.
[19] J. Wu, W. Wang, H. Cai, Research on fuzzy adaptive control of LLC resonant converter. J. China Univ. Metrol. 2017, 28(02): 196-202.
[20] Z. U. Zahid, Z. M. Dalala, R. Chen, et al. Design of bidirectional DC–DC resonant converter for vehicle-to-grid (V2G) applications IEEE T. Trans. Electrif. 2015, 1(3): 232-244.
[21] Z. R. Jiang, P. C. Zhao, A review of small-signal modeling methods for LLC resonant converters. Electron. Fabr. 2023, 31(20): 22-24+18. DOI: 10.16589/j.cnki.cn11-3571/tn.2023.20.026.
[22] X. M. Gao. Research on high efficiency LLC resonant converter. Hangzhou: Zhejiang University, 2015.
[23] Z. Gao. Scaling and bandwidth-parameterization based controller tuning, IEEE. Proceedings of the 2003 American Control Conference. Denver, USA: IEEE Press, 2003: 4989-4996.